Journal of Applied Fluid Mechanics, Vol. 18, No. 2, pp. 389-398, 2025.
Available online at www.jafmonline.net, ISSN 1735-3572, EISSN 1735-3645.
https://doi.org/10.47176/jafm.18.2.2883

Effect of Height on the Supersonic Flow over a Blunt Vertical Fin

D. Sahoo[1†], S. T. Kansara[2] and P. Kumar[3]

[1]*Department of Aerospace Engineering, Graphic Era (Deemed to be University), Dehradun-248002, India*
[2]*Department of Aerospace Engineering, MIT Art, Design and Technology University, Pune-412201, India*
[3]*Department of Space Engineering and Rocketry, Birla Institute of Technology, Mesra, Ranchi- 835215, India*

†*Corresponding Author Email: devabratasahoo.ae@geu.ac.in*

ABSTRACT

Understanding how protrusions, such as fins attached to flat or streamlined bodies, affect aerodynamics, especially in high-speed contexts, is vital for aerospace applications. These protrusions significantly influence overall aerodynamics and require a comprehensive understanding for accurate analysis and prediction of aerodynamic performance. This understanding is particularly critical in supersonic flight, where even minor aerodynamic disturbances can impact vehicle stability and efficiency. Therefore, a thorough understanding of protrusion-induced flow phenomena is essential for advancing aerospace engineering and improving supersonic vehicle performance and safety. The present paper focuses on the complex supersonic flow over a vertical fin, using a combination of experimental and computational methods. The study aims to understand how variations in fin height influence the behavior of the Lambda shock and any resulting changes in shock length. Specifically, the paper investigates different fin height-to-diameter (H/D) ratios ranging from 0.5 to 1.5 in steps of 0.25. To achieve this, both experimental testing in a supersonic wind tunnel and numerical simulations using the commercial CFD tool ANSYS-FLUENT are employed. Through this dual approach, the paper seeks insights into the characteristics of the Lambda shock and its effects on key aerodynamic parameters, such as shock strength and drag coefficient. By thoroughly investigating these aspects, the paper contributes to a deeper understanding of the complex flow phenomena associated with supersonic flow over vertical fins, potentially guiding the design and optimization of aerospace vehicles. The outcomes indicate that a fin height of 12 mm (H/D=1.0) provides the best balance in terms of pressure distribution, Lambda shock length, and drag coefficient, making it the optimal choice for enhancing aerodynamic stability and performance in supersonic conditions.

Article History

Received June 1, 2024
Revised September 2, 2024
Accepted September 5, 2024
Available online December 4, 2024

Keywords:

Protrusions
Vertical fin
Aerodynamics
Experimental testing, Supersonic flow
Aerospace applications
Flow-phenomena

1. INTRODUCTION

The impact of protrusions like vertical fins on aircraft and missiles becomes increasingly significant at supersonic speeds, where they induce complex flow phenomena such as shock waves and expansion fans. These interactions alter pressure, temperature, and velocity distributions around the fin, affecting the vehicle's stability and efficiency. Accurate analysis of these effects is crucial for optimizing aerodynamic performance. This study explores how changes in fin height influence the Lambda shock and other aerodynamic parameters. By combining experimental wind tunnel tests with computational simulations using ANSYS-FLUENT, the research aims to provide insights into supersonic flow dynamics, guiding the design and performance optimization of supersonic vehicles by addressing factors like drag, heat transfer, and structural loads.

Figure 1 depicts flow around a blunt fin on a flat plate, showing the complex flow physics involved. After the bow shock wave when the flow hits the fin, it creates a stagnation point on the central streamline where the velocity is zero. The flow then splits and moves around the sides of the fin, causing expansion zones at the fin's corners. Thus, the interaction of the flow with the blunt fin results in a bow shock, stagnation point and expansion zone, around the vertical fin.

Ching-Mao Hung et al. (1985) simulated supersonic flow over a blunt fin, matching surface pressure data and emphasizing the horseshoe vortex, though mesh limitations

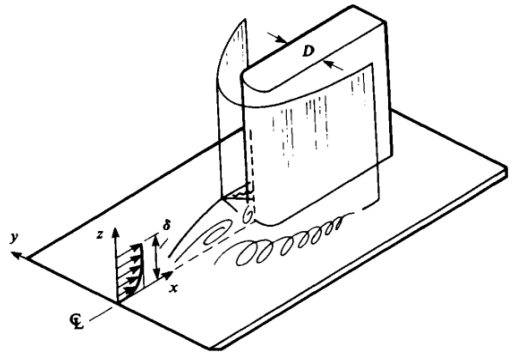

Fig. 1 Blunt fin over a flat plate (Hung et al. 1985)

affected shock resolution, indicating a need for further studies on heat transfer and turbulence models. Knight & Badekas (1992) analyzed the interaction of a swept oblique shock with a turbulent boundary layer from a 20-degree fin at Mach 4, using Reynolds-averaged Navier-Stokes equations. Narayan et al. (2017) compared hypersonic flows around blunted and parabolic nose cones, finding that parabolic cones with higher fineness ratios offered better drag reduction and lower heating. Fox et al. (2012) studied separated flow upstream of a blunt fin in hypersonic flow, highlighting oscillatory behavior and quasi-steady viscous interaction. Wang et al. (1998) examined turbulent separation induced by a blunt fin at Mach 7.8, noting distinct interaction regions, unsteady shock motion, and double peaks in wall pressure and heat transfer. Kolesnik & Smirnov (2023) investigated temperature ratio effects on supersonic flow past a blunt fin, revealing dual solutions useful for flow control. Song et al. (2007) studied heat transfer near sharp and blunt fins in supersonic flow, finding higher heat transfer coefficients for sharp fins and correlating values to wedge angle. Kolesnik & Smirnov (2024) simulated laminar supersonic flow past a blunt fin/plate junction, identifying dual stable solutions within a critical Reynolds number range. Poggie & Smits (1997) used continuous wavelet transform to analyze wall-pressure fluctuations in a Mach 3 flow over a blunt fin, identifying time scales for turbulence and shock crossing. Dolling & Bogdonoff (1982) found blunt fin-induced shock wave turbulent boundary layer interactions caused r.m.s. pressure peaks up to 40 times higher than the incoming boundary layer. Ablaev et al. (2000) examined localized disturbances in a separation bubble, showing rapid turbulence transition at low Reynolds numbers and discrepancies between experimental and CFD results. Dolling & Bogdonoff (1979) investigated 3-D shock wave turbulent boundary layer interactions, analyzing turbulent boundary layer thickness and unsteady shock wave structures at Mach 3. Dolling & Bogdonoff (1980) studied 3-D shock wave turbulent boundary layer interactions, revealing scaling insights under varying turbulent boundary layer thickness ratios at Mach 3. Hale (2014) investigated conical shock wave interactions with a compressible turbulent boundary layer at Mach 2.05, revealing flow separation and vortical structure dynamics. Weng et al. (2024) found new interaction phenomena in Mach 2.2 between conical shock waves and axisymmetric boundary layers, establishing a novel interaction model. Seynet & Kitchens Jr (1977) proposed a correlation for primary separation distance in supersonic turbulent boundary layers around cylindrical obstacles, with deviations within 25%. Viswanath (1988) reviewed 2D shock-wave-turbulent-boundary-layer interactions at high speeds, highlighting turbulence dynamics and control techniques. Dolling et al. (1977) suggested an inviscid character for 3-D shock wave turbulent boundary layer interactions, challenging traditional scaling laws. Kolesnik & Smirnov (2021) found two stable solutions for supersonic laminar flow over a blunt fin, with vortex configurations dependent on Reynolds number. Mortazavi & Knight (2017) validated numerical simulations for heat transfer in Mach 14 hypersonic flows past a blunt fin-plate junction with experimental data. Kolesnik & Smirnov (2023) revealed two stable solutions for supersonic flow past a blunt fin, indicating meta-stable flow states and critical Reynolds numbers. Kolesnik & Smirnov (2024) found that negative angles on a blunt fin's leading edge lead to dual stable flow solutions, transitioning to a single solution beyond 7.5° to 10° skew angle. Ngoh & Poggie (2022) found large-scale unsteadiness in Mach 3 turbulent flow over a blunt fin modulated by time-periodic forcing, suggesting flow control opportunities. Dolling & Brusniak (1993) revealed fluctuating wall pressure in a Mach 5 turbulent boundary layer over a blunt fin, predicting standard deviation locations and unsteady shock foot behavior. Guo et al. (2016) simulated fluid-thermal interactions on hypersonic blunt bodies, showing longer spikes decrease drag coefficient by 5.7% and highlighting the need for coupled analysis. Xiao et al. (2018) found that increasing bluntness of V-shaped leading edges negatively affects thermal protection, with heat flux up to 24 times stagnation-point value. Berry et al. (1999) found that X-33 vehicle aeroheating predictions matched wind tunnel data, validating thermal protection system development. Hollis et al. (2001) confirmed that X-33 aeroheating predictions agreed with wind tunnel data. Horvath et al. (2001) used phosphor thermography to study hypersonic aeroheating on X-33 models, revealing shock/shock interactions and accurate laminar windward heating extrapolation. Berry et al. (2001) investigated X-33 boundary layer transition, revealing transition pattern variations and effects of discrete roughness and bowed panels on the aft-body surface. Berry et al. (1999) conducted hypersonic aeroheating tests for the X-34, demonstrating laminar, transitional, and turbulent boundary layers and supporting the Thermal Protection System design.

Previous studies have extensively explored various aspects of supersonic flows over fins, including shock wave interactions, heat transfer, flow separation, temperature effects, and turbulence. However, these studies often did not address how different fin heights specifically influence supersonic flow characteristics. The realistic motivation for the present study was to solve specific aerodynamic challenges encountered in supersonic flight, particularly in reducing drag and improving stability by optimizing fin height. Present study fills this gap by examining how varying fin height impacts pressure distribution, shock length, and drag both

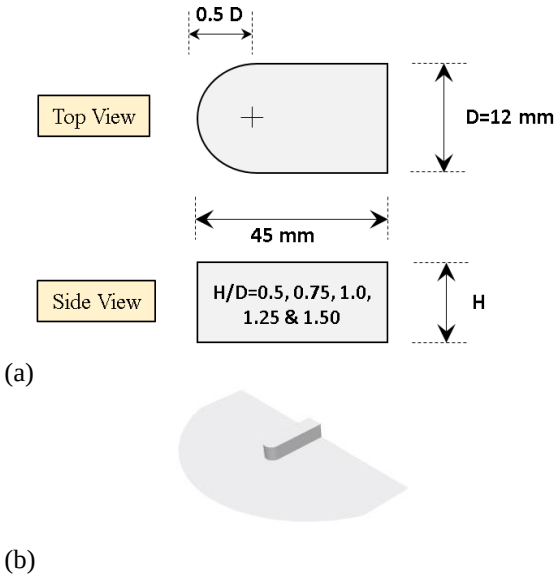

Fig. 2 a) Geometrical details of the fin (top view and side view of the blunt fin), b) Isometric view of the vertical blunt fin with base plate

computationally and experimentally offering novel insights into flow control.

2. RESEARCH METHODOLOGY

2.1 Model Geometry

The blunted fin geometry comprises of a rectangular structure with a blunted semicircular cross section at the beginning, intended for analysis in a three-dimensional domain. When viewed from the top, the fin exhibits a length of 45 mm and a width of D=12 mm, with the radius of the blunted semicircle measuring half the width at 6 mm (0.5D). From the side view, the height of the fin varies relative to its width, spanning ratios of H/D= 0.5, 0.75, 1.0, 1.25, and 1.50. Mounted on a base plate the blunted fin features a rectangular body and a rounded cross-section at the beginning, presenting a flexible framework for studying aerodynamic characteristics and flow phenomena of a blunted vertical fin at different H/D when subjected to a supersonic flow of Mach 2. The detailed geometry of the fin is shown below in Fig. 2a. The three-dimensional isometric view of the adopted fin is shown in Fig. 2b.

2.2 Experimental Methodology

The blowdown type Supersonic Wind Tunnel at Birla Institute of Technology, Mesra, Ranchi, India having a test section size of 50mmx100mm was utilized to perform all the experiments. The experiments were carried out at a fixed Mach number of 2.0, with settling chamber total pressure of about 3.2 bar, which was measured using a pressure transducer (Make Sensym, Model ASCX150DN), and Reynolds number (Re) of $3.5x10^5$ based on the base diameter of the model. The vertical fin was mounted on the side wall plate of the test section. The arrangements were made such that, the flow over the base plate with the vertical fin mounted over it can be easily analyzed experimentally using suitable

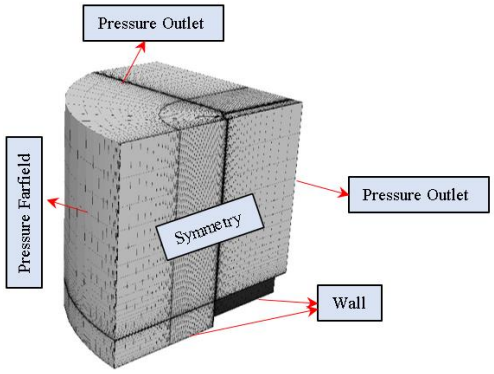

Fig. 3 Detailed mesh and boundary types adopted for the CFD simulations

pressure measurements and flow visualizations. A 16 channel Pressure scanner was adopted to measure the centerline wall pressure of the base plate whereas the surface flow field was visualized using oil flow visualization technique. The above mentioned experimental methodology was utilized on the test case of H/D = 1.0 and the experimental data obtained has been adopted to validate the computational solver. The details of the computational methodology adopted in the present research and solver validation details have been briefed in the following section.

2.3 Computational Methodology

In the current work, steady state Reynolds Averaged Navier Stokes Equations are numerically solved, employing a time-averaged and density-based approach. A K- ω SST turbulence model with a second-order explicit formulation is implemented to capture the flow physics accurately. The k-ω SST turbulence model is used for its accuracy in capturing complex turbulence behaviors in high-speed flows, crucial for analyzing supersonic flow over a vertical fin and its impact on the Lambda shock phenomenon. The computational mesh and boundary conditions adopted for validation is explained in the sub-sections followed by the validation and grid independence test, ensuring the reliability and accuracy of the computational simulations.

2.3.1 Meshing and Boundary Conditions

Figure 3 presents a depiction of the detailed mesh structure and the types of boundaries utilized for the validation process. The numerical simulations were conducted under conditions of a freestream Mach number of 2, with a static pressure of 39408.56 Pa and a static temperature of 166.67 K corresponding to a freestream Reynolds number of $3.5x10^5$ based on the base diameter of the model.

Furthermore, Fig. 4 provides an open perspective of the three-dimensional grid specifically generated for the computational fluid dynamics (CFD) simulation. This visualization offers insight into the complexity of the grid structure. Moreover, Fig. 5 illustrates the grid topology at the symmetry plane, offering a clear understanding of the computational domain's discretization. These visual

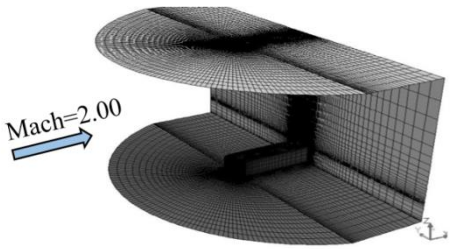

Fig. 4 Open view of 3D grid generated for CFD Simulations

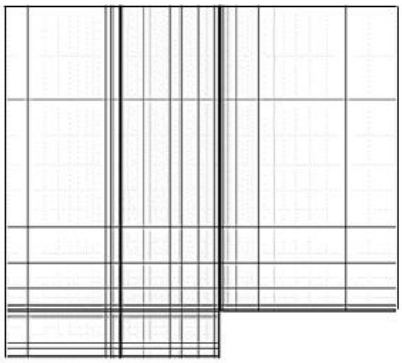

Fig. 5 Grid Topology at Symmetry Plane

representations are crucial for ensuring the accuracy and reliability of the numerical results.

The boundaries of the computational domain include Pressure Farfield, representing the upstream boundary; Pressure Outlet, representing the freestream boundary and top boundary where the flow exits the domain. The vertical fin along with the base is represented by no slip wall boundary type. In order to reduce the total cell count and computational time, symmetry boundary type has been adopted at the mid plane of the computational domain.

2.3.2 Validation and Grid Independence Test

The computational data and results have been meticulously validated against the experimental findings of the case of H/D=1.0 and showcased in Fig. 6. By comparing the variation in the centerline wall pressure distribution measured upstream of the blunted fin, a fair agreement with the experimental observations was observed. Moreover, a grid independence test has been conducted, to maintain a wall Y+ over fin of less than 5 throughout the computations. Table 1 summarizes the details of grid density and corresponding Wall Y+ values used in the computational simulations. Three grid densities, namely Coarse (0.4 million cells), Medium (0.6 million cells), and Fine (0.8million cells), were employed and the fine grid ensured a Wall Y+ value of less than 5 and hence was adopted for the present research. Furthermore, Fig. 7 provides additional insight into the validation process by presenting a qualitative comparison of oil flow visualization obtained from both experiment and computation. Upstream of the vertical fin,

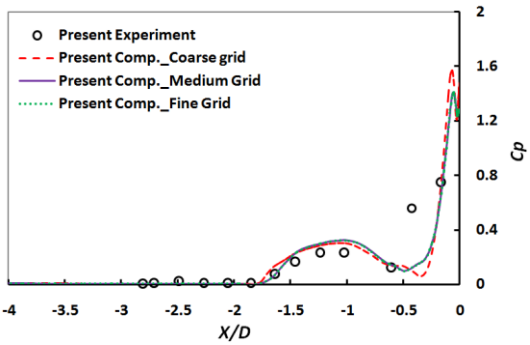

Fig. 6 Comparison of centerline wall pressure distribution measured and computed upstream of the blunted fin

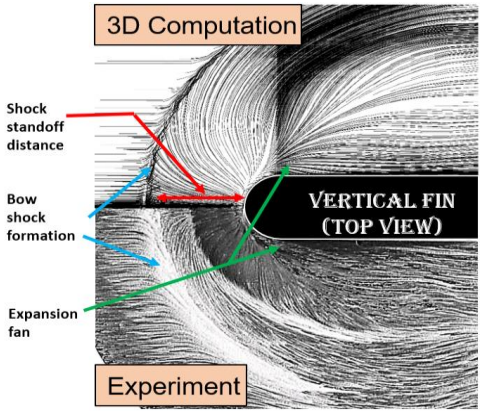

Fig. 7 Qualitative validation: comparison of oil flow visualization obtained from experiment and computation

Table 1 Details of Grid density and Wall Y+ values

Grid	Cell count	Wall Y+
Coarse	0.4 million	below 12
Medium	0.6 million	below 10
Fine	0.8 million	below 5

both computational and experimental studies reveal the formation of a bow shock. This shock wave is created as the supersonic flow encounters the fin, resulting in a distinct bow-shock pattern around it. The shock standoff distance, or the distance between the bow shock and the surface of the fin, is observed to be consistent in both simulation and experimental observations. Additionally, an expansion fan is noted in this region, where the flow undergoes a series of expansion waves as it interacts with the fin's geometry. These phenomena are integral in understanding the aerodynamic effects on the vertical fin and are consistently captured in both computational analyses and physical experiments.

3. RESULTS AND DISCUSSIONS

The flow phenomena behind the Lambda shock exhibit notable characteristics, as observed in the centerline wall pressure distribution measured upstream of the blunted fin (illustrated in Fig. 8). Initially, a bow shock forms at the

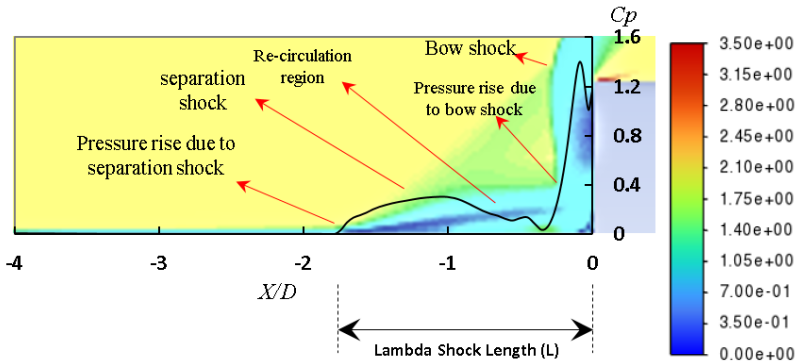

Fig. 8 Flow Physics of Lambda Shock for the case of a typical vertical fin

tip of the blunted fin, inducing a discernible pressure increase. This bow shock arises from the sudden deceleration of the oncoming flow, leading to compression and elevated pressure levels. The bow shock occurs as the airflow encounters the leading edge of the blunted fin, causing a rapid increase in pressure due to compression. As the bow shock weakens, a recirculation region emerges, resulting in the development of a separation shock. The recirculation region is characterized by a swirling motion of the flow, where streamlines reverse direction, creating a pocket of low-pressure air. This separation shock marks the point where the flow detaches from the surface of the fin due to adverse pressure gradients, resulting in a sudden drop in pressure. A separation shock occurs when the boundary layer of airflow separates from the surface of an object, creating a region of low pressure rise. In this case, the separation shock forms as the airflow separates from the surface of the blunted fin, leading to a sudden decrease in pressure downstream.

Downstream of the separation shock, another pressure rise is observed. This phenomenon is attributed to the interaction between the detached flow and the oncoming freestream, causing further compression and an increase in pressure along the centerline. The complex interplay of these flow phenomena offers valuable insights into the aerodynamic behavior of supersonic flow over blunted fins. By unraveling the intricate dynamics one can fine-tune aerodynamic designs to optimize performance and stability in high-speed flight regimes.

These sequential events highlight the intricate interplay between shock waves and the flowfield, leading to varying pressure distributions along the centerline upstream of the blunted fin. A comprehensive analysis of these phenomena will delve into variations in the length of the Lambda shock with height, changes in the variation of drag coefficient with height, and fluctuations in peak pressure coefficient or shock strength with height. Such detailed insights are crucial for optimizing the design and performance of aerodynamic surfaces in hypersonic flow environments, enabling more efficient and stable aerospace vehicle configurations.

3.1 Effect of Fin Height on the Flowfield

The Mach contour visualization as shown in Fig. 9 provides crucial insights into the aerodynamic behavior of a blunt fin in supersonic flow. The formation of the bow

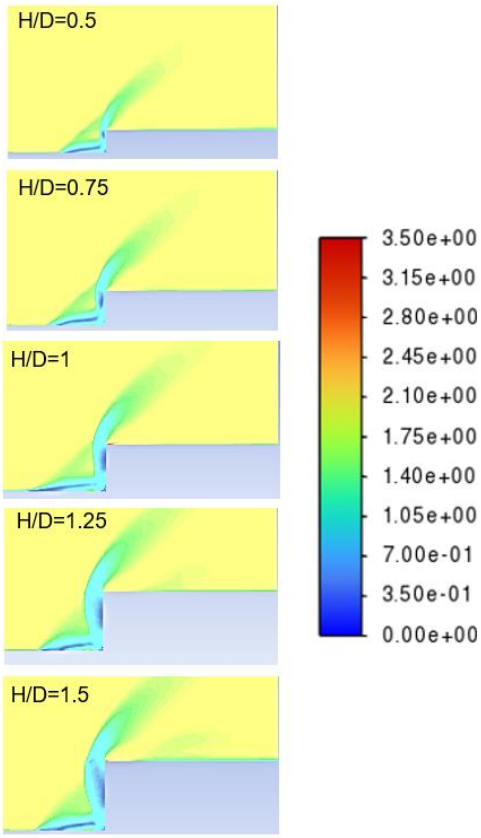

Fig. 9 Mach contours representing variation in lambda shock for different fin height to diameter ratios (H/D= 0.5, 0.75, 1, 1.25, 1.75)

shock at the fin's leading edge signifies the abrupt deceleration of supersonic airflow, inducing compression, elevated pressure, and temperature. This alteration in flow significantly impacts aerodynamic performance, contributing to drag and thermal stresses. As airflow separates from the fin's surface and accelerates, a shock wave forms, depicted in the Mach contour visualization by a shift in colors. This abrupt color change indicates the rapid pressure and temperature increase associated with the shock wave's formation.

As the height of the blunt vertical fin increases in supersonic flow, several factors contribute to the intensification of the bow shock ahead of the fin. Firstly, the increased height of the fin results in a larger surface area for interaction with the airflow. This larger surface

area creates more opportunities for the airflow to be compressed, leading to a more significant buildup of pressure ahead of the fin. Consequently, the bow shock becomes more pronounced as it forms to accommodate this increased pressure differential between the airflow and the fin surface. Secondly, the increased height allows for a greater volume of airflow to be deflected around the fin. As the airflow is forced to navigate around the larger surface area of the taller fin, it undergoes more significant changes in direction and velocity. This increased deflection of airflow contributes to a more intense compression effect, further enhancing the formation and strength of the bow shock. Additionally, the higher fin height extends the region over which the airflow is influenced by the fin's presence. This prolonged interaction zone provides more time and space for the airflow to adjust to the fin's presence, resulting in a more gradual but sustained increase in pressure leading up to the bow shock.

In summary, the intensification of the bow shock with increasing height of the blunt vertical fin in supersonic flow is attributed to the combined effects of increased surface area for compression, enhanced airflow deflection, and prolonged interaction between the fin and the airflow. These factors lead to a more pronounced and intense bow shock, as observed in the trend of Mach contours.

3.2 Impact of Blunt Fin Height on Shock Wave Formation and Flow Separation in Supersonic Flow

Figure 10 showcases the shock streamlines for three different fin heights (H = 6 mm, H = 12 mm, and H = 18 mm) in a supersonic flow, highlighting the impact of fin height on shock wave formation and flow separation patterns.

For the smallest fin height of 6 mm (H/D=0.5), the bow shock that forms at the leading edge of the fin is relatively weak. This weak bow shock indicates a moderate increase in pressure as the supersonic flow encounters the fin. Downstream of this initial shock, a small recirculation zone forms. This zone is characterized by a reversed flow direction and a pocket of low-pressure air, indicating minor flow separation. The flow reattaches to the surface shortly after the fin, resulting in simpler shock patterns and a less complex streamline structure.

When the fin height is increased to 12 mm (H/D=1), the bow shock becomes more pronounced. This stronger bow shock is a result of the larger surface area of the fin interacting with the oncoming flow, leading to a higher pressure rise. Behind the fin, the recirculation region is larger compared to the 6 mm fin, indicating a more significant separation shock. This larger recirculation zone suggests that the flow separates more substantially from the surface of the fin, creating a wider area of reversed flow. Consequently, the flow reattaches further downstream, and the shock patterns become more complex, with intricate streamline contours reflecting the interaction between the detached flow and the freestream.

At the tallest fin height of 18 mm (H/D=1.5), the bow shock is the most intense among the three cases. This intense bow shock signifies a significant increase in pressure and temperature at the leading edge of the fin.

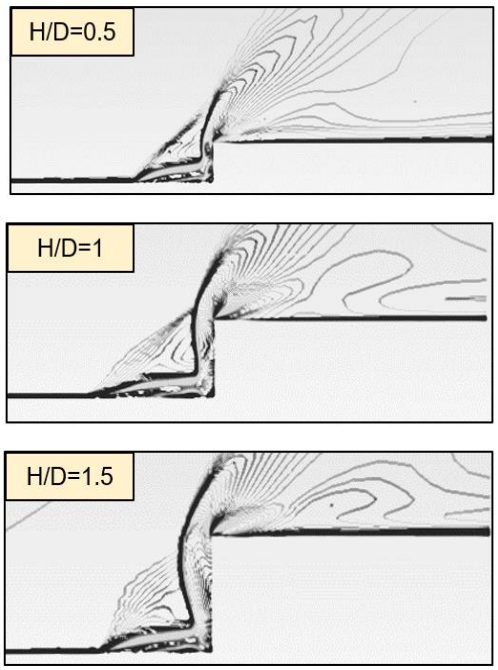

Fig. 10 Streamlines representing the impact of Blunt Fin height to diameter ratios on Shock Wave Formation and Flow Separation in Supersonic Flow

The recirculation zone behind the fin is the largest, indicating a substantial separation shock. The flow separation is extensive, and the reversed flow region is broad and more pronounced. The streamline patterns are highly complex, with multiple reattachment points and intricate shock interactions. These patterns reflect significant turbulence and variations in pressure gradients, resulting in an elaborate flow structure.

As the height of the blunt fin increases, the intensity of the bow shock also increases. This is due to the larger surface area presented by the higher fin, which causes a greater disruption to the supersonic flow. Correspondingly, the height of the blunt fin leads to larger recirculation zones, as the increased height causes more substantial flow separation, resulting in wider and more complex regions of reversed flow. The complexity of the shock streamline patterns grows with the height of the blunt fin, with taller fins inducing more intricate interactions between the shock waves and the flow field. This results in more elaborate streamline contours, reflecting the intricate interplay between shock waves and aerodynamic surfaces in high-speed environments.

Overall, the figure effectively illustrates the significant impact of the height of the blunt fin on the formation and behavior of shock waves in supersonic flow, highlighting the relationship between increased fin height and the resulting aerodynamic phenomena.

3.3 Impact of Blunt Fin Height on Centerline Pressure Distribution

Figure 11 depicts the coefficient of pressure (Cp) distribution along the centerline upstream surface of a blunt vertical fin for different heights: 6mm, 9mm, 12mm, 15mm, and 18mm. The x-axis shows the non-dimensional distance (X/D) along the fin surface,

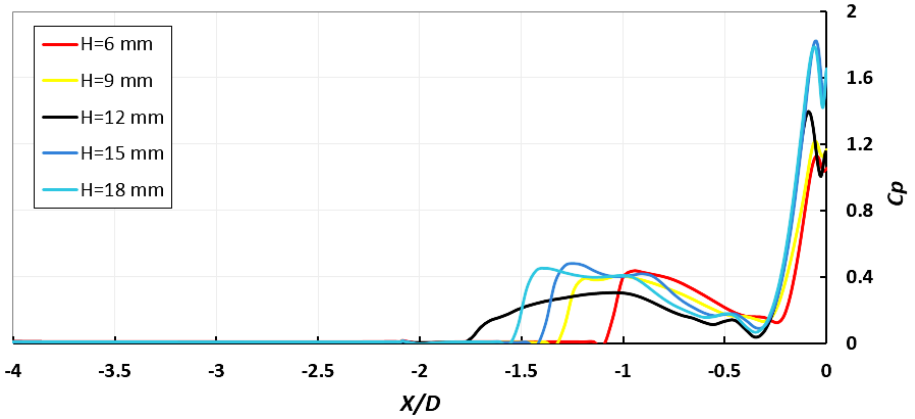

Fig. 11 Coefficient of Pressure Distribution along Blunt Vertical Fin Upstream Surface at Various Heights

while the y-axis represents the coefficient of pressure Cp. As the height increases, several notable trends are observed: For the smallest height (H = 6mm), the Cp rises sharply near X/D = -0.5, indicating a weaker shock and less intense flow separation. At H = 9mm, the peak Cp is slightly higher and the rise is more gradual, suggesting a stronger interaction with the shock and greater pressure build-up. When H = 12mm, the Cp peak shifts downstream and becomes higher, indicating stronger shock formation and separation effects. For H = 15mm and 18mm, the Cp distribution shows multiple peaks and the highest values, suggesting complex shock interactions.

The trends in Cp distribution are influenced by the height of the fin, which affects the aerodynamic interaction between the shock waves and the boundary layer. As the fin height increases, the interaction surface area also increases, leading to stronger shocks and more complex flow separation and reattachment patterns. Higher fins create more pronounced flow disturbances, resulting in higher pressure gradients and multiple peaks in the Cp distribution.

Figure 12 shows the variation of lambda shock length (L) with the height (H) of the blunt vertical fin. The shock length initially increases from H = 6mm to H = 12mm, indicating that the shock wave structure elongates as the height increases. However, there is an abrupt decrease in L from H = 12mm to H = 15mm, followed by a resurgence from H = 15mm to H = 18mm. The initial increase in lambda shock length is due to the larger frontal area presented by the taller fin, which interacts more extensively with the incoming flow, creating a longer shock structure. The sudden decrease between H = 12mm and H = 15mm suggests a complex change in shock interaction dynamics, possibly due to boundary layer transition or changes in shock wave reflection patterns. The resurgence in shock length beyond H = 15mm indicates that the flow stabilizes again, allowing the shock structure to elongate once more. These fluctuations reflect the intricate interplay between the shock waves and boundary layer at different heights. The length of the Lambda shock significantly impacts the stability of the vehicle during supersonic flight. A longer Lambda shock, indicating a more extensive separation region and stronger shock interaction, enhances aerodynamic stability by exerting greater control over the surrounding flow field.

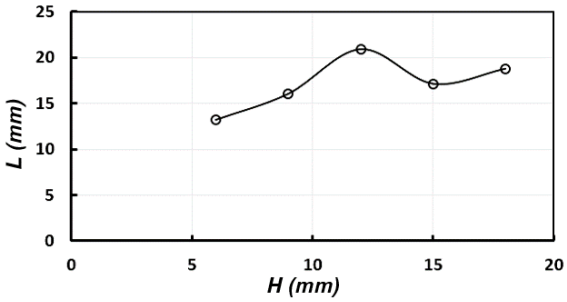

Fig. 12 Variation of Lambda Shock Length with Height of Vertical Blunt Fin

This extended shock structure modifies the pressure distribution around the fin, promoting a more stabilized flow pattern and reducing the risk of flow separation and associated instabilities. Conversely, a shorter Lambda shock signifies weaker shock control and inadequate interaction with the flow field, leading to potential instabilities such as boundary layer separation and vortex shedding. Optimizing the length of the Lambda shock is therefore crucial for maintaining aerodynamic stability and ensuring safe and efficient operation in high-speed environments. However, this abrupt change (decrease) in the lambda shock length upon change in H from 12 to 15 needs an in-depth study.

Figure 13 illustrates the ratio of lambda shock length to fin height (L/H) against the height (H) of the vertical blunt fin. The ratio decreases as the height increases, showing that the efficiency of height in extending the lambda shock length diminishes with increasing fin height. At smaller heights, the ratio L/H is higher, indicating that shorter fins are more efficient in producing a longer lambda shock length relative to their size. As the height increases, the additional height contributes less effectively to extending the shock length due to more complex interactions out of which boundary layer transitions might be one of the reasons. These effects reduce the efficiency of height in proportionally increasing the lambda shock length. The decreasing trend in L/H ratio suggests that while taller fins can generate longer shock structures, the incremental benefit per unit height decreases, indicating a diminishing return on aerodynamic efficiency as the fin height grows.

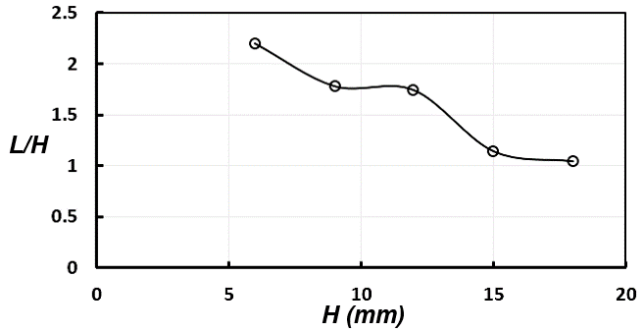

Fig. 13 Variation of Lambda Shock Length/Height with Height of Vertical Blunt Fin

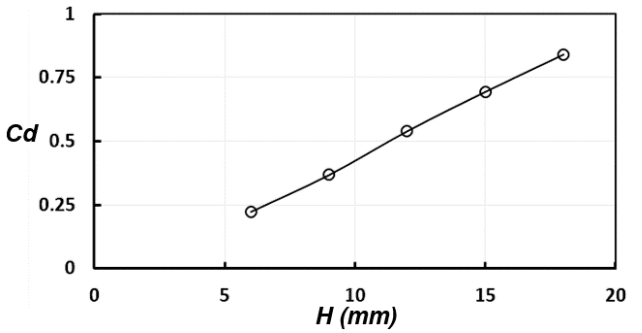

Fig. 14 Plot of variation of the coefficient of drag with different heights of the blunt vertical fin

Figures 11, 12, and 13 reveal the complex aerodynamic behavior of blunt vertical fins at varying heights, showing changes in pressure distribution, non-linear shock length variation, and diminishing height efficiency. These insights are crucial for optimizing fin design and improving aerodynamic performance and stability in high-speed flows.

3.4 Coefficient of Drag

The variation of the coefficient of drag with different heights of the blunt vertical fin, as depicted in Fig. 14 and corroborated by the data presented in Table 2, reveals a notable trend: a linear increase in the drag coefficient with an increase in fin height. This trend signifies the escalating resistance encountered by the fin as its height extends, pointing towards significant implications for the aerodynamic performance of the system

One prominent factor contributing to this observed trend is the augmented surface area presented by a taller fin. As the fin's height increases, so does its surface area available for interaction with the airflow. This expanded surface area results in a greater frictional drag experienced by the fin as the airflow passes over and around it. Consequently, the drag force acting on the fin amplifies proportionally with the heightened surface area, leading to the linear increase in the drag coefficient. Moreover, the escalating height of the blunt vertical fin also exacerbates the likelihood of flow separation occurring. Flow separation, characterized by the airflow detaching from the fin's surface, creates recirculation zones and turbulent airflow, which significantly contribute to increased drag. With taller fins, the probability of encountering flow

Table 2 Computed aerodynamic drag coefficients for different heights of the blunt vertical fin

H (mm)	H/D	Drag coefficient
6	0.5	0.2236
9	0.75	0.3682
12	1	0.5401
15	1.25	0.6949
18	1.5	0.8411

separation rises due to alterations in pressure distribution and flow behavior along the fin's surface, further augmenting the drag coefficient. Additionally, the taller fin generates a larger wake region downstream, where the airflow becomes turbulent and chaotic. This wake region intensifies with increasing fin height, exacerbating the drag forces acting on the fin. The turbulent airflow within the wake interacts with the surrounding fluid, inducing additional drag forces on the fin and accentuating the linear increase in the drag coefficient. Furthermore, alterations in pressure distribution around the taller fin contribute to changes in pressure differentials, which also influence the aerodynamic forces acting on the fin. As the height increases, these alterations in pressure distribution can magnify the drag forces experienced by the fin, further reinforcing the observed trend of linearly increasing drag coefficient with increasing fin height.

In summary, the linear increase in the drag coefficient with increasing height of the blunt vertical fin is a consequence of several interrelated factors, including the augmented surface area, flow separation phenomena, wake formation, and alterations in pressure distribution. Understanding and mitigating these aerodynamic effects are crucial for optimizing the design and performance of vertical fin configurations in supersonic and hypersonic flow regimes.

4. CONCLUSION

Based on the analysis, the optimal height to diameter ratio for the blunt vertical fin that provides better aerodynamic performance is H/D = 1. This height offers a balanced performance across the key aerodynamic parameters: pressure distribution, length of the Lambda shock, and drag coefficient.

Pressure Distribution: At H/D = 1, the pressure coefficient (Cp) distribution shows a moderate peak that is neither too sharp nor too gradual. This indicates a well-managed interaction with the shock and a balanced pressure build-up, which is crucial for maintaining aerodynamic stability and avoiding excessive pressure gradients that could lead to flow separation.

Length of the Lambda Shock: The Lambda shock length at H/D = 1 is sufficient to provide strong shock control and extensive interaction with the flow field. This extended shock structure helps to stabilize the vehicle by promoting a smoother flow pattern and reducing the likelihood of boundary layer separation. Height to diameter ratios lower than H/D = 1 result in shorter Lambda shocks, which provide inadequate control and can lead to instability. Conversely, height to diameter ratios

higher than H/D = 1, particularly H/D = 1.25 and H/D = 1.5, exhibit fluctuations in the shock length, indicating complex and less predictable shock interactions that can compromise stability.

Drag Coefficient: The drag coefficient increases linearly with fin height. At H/D = 1, the drag is manageable and significantly lower compared to taller fins with H/D = 1.25 and H/D = 1.5, which experience substantial drag due to larger surface areas and more pronounced flow separation. Lower height to diameter ratios, such as H/D = 0.5 and H/D = 0.75, while having lower drag, do not provide adequate shock control and stability benefits.

Therefore, H/D = 1 is optimal as it achieves a balance by offering sufficient shock length for stability, manageable pressure distribution for smooth flow, and a reasonable drag coefficient for efficient aerodynamic performance. Other height to diameter ratios are eliminated due to their inability to provide this balanced performance, either by causing excessive drag, insufficient shock control, or complex pressure distributions that compromise stability.

In conclusion, the study underscores the importance of carefully selecting the height to diameter ratios of protrusions in supersonic flow applications, emphasizing the need for a nuanced understanding of the trade-offs between aerodynamic performance, stability, and drag. By optimizing protrusion height, aerospace engineers can enhance the efficiency and effectiveness of high-speed vehicles, advancing the frontiers of aerospace technology.

CONFLICT OF INTEREST

The authors declare that there are no financial or non-financial interests in this study. Furthermore, the authors have no conflicts to disclose.

AUTHORS CONTRIBUTION

Devabrata Sahoo and **Sakshi Tushar Kansara** conducted the numerical simulations and prepared the manuscript. **Priyank Kumar** and **Devabrata Sahoo** conducted the experiment. **Priyank Kumar** supervised the work and proof read the manuscript. All the authors discussed the results and contributed to the article.

REFERENCES

Ablaev, A. R., Dovgal, A. V., Grek, G. R., Katäsonov, M. M., & Kozlov, V. V. (2000). *Experimental investigation of localized disturbances in a separation bubble*. Proceedings of the International Conference on the Methods of Aerophysical Research (Part 1). https://apps.dtic.mil/sti/pdfs/ADA382160.pdf#page=7

Berry, S. A., Horvath, T. J., DiFulvio, M., Glass, C., & Merski, N. R. (1999). X-34 experimental aeroheating at Mach 6 and 10. *Journal of Spacecraft and Rockets*, *36*(2), 273–279. https://doi.org/10.2514/2.3447

Berry, S. A., Horvath, T. J., Hollis, B. R., Thompson, R. A., & Hamilton II, H. H. (2001). X-33 hypersonic boundary layer transition. *Journal of Spacecrafts and Rockets*, *38*(5). https://doi.org/10.2514/2.3748

Dolling, D. S., & Bogdonoff, S. M. (1979). Investigation of three-dimensional shock wave turbulent boundary layer interaction: An exploratory study of blunt fin-induced flows. *AIAA Journal*, *55*(2), 133–140. https://doi.org/10.2514/1.J055283

Dolling, D. S., & Bogdonoff, S. M. (1980). *Experimental study of three-dimensional shock wave turbulent boundary layer interaction: Scaling of sharp and blunt fin-induced flowfields*. Defence Technical Research Center, Naval Surface Weapons Center, White Oak Laboratory. ADA086875. https://apps.dtic.mil/sti/pdfs/ADA086875.pdf

Dolling, D. S., & Bogdonoff, S. M. (1982). *An experimental investigation of the unsteady behavior of blunt fin-induced shock wave turbulent boundary layer interactions.* Proceedings of the 14th Fluid and Plasma Dynamics Conference. https://doi.org/10.2514/6.1981-1287

Dolling, D. S., & Brusniak, L. (1993). *Flowfield dynamics in blunt fin-induced shock wave/turbulent boundary layer interactions* (NASA Grant NAG3-1023). https://ntrs.nasa.gov/api/citations/19940023299/downloads/19940023299.pdf

Dolling, D. S., Cosad, C. D., & Bogdonoff, S. M. (1977). *Three-dimensional shock wave turbulent boundary layer interactions: A preliminary analysis of blunted fin-induced flows*. Naval Surface Weapons Center. ADA046317. https://apps.dtic.mil/sti/pdfs/ADA046317.pdf

Fox, J. S., O'Byrne, S., Houwing, A. F. P., Papinniemi, A., Danehy, P. M., & Mudford, N. R. (2012). Fluorescence visualization of the hypersonic flow establishment over a blunt fin. *AIAA Journal*, *39*(7), 1254–1261. https://doi.org/10.2514/2.1451

Guo, S., Xu, J., Qin, Q., & Gu, R. (2016). Fluid–thermal interaction investigation of spiked blunt bodies at hypersonic flight condition. *Journal of Spacecraft and Rockets*, *53*(4), 705–714. https://doi.org/10.2514/1.A33370

Hale, J. T. (2014). *Interaction between a conical shock wave and a plane compressible turbulent boundary layer at Mach 2.05* [Thesis, University of Illinois at Urbana-Champaign]. Retrieved from https://hdl.handle.net/2142/72992

Hollis, B. R., Horvath, T. J., Berry, S. A., Hamilton II, H. H., & Alter, S. J. (2001). X-33 computational aeroheating predictions and comparisons with experimental data. *Journal of Spacecraft and Rockets*, *34*(5), 702–710. https://doi.org/10.2514/2.3751

Horvath, T. J., Berry, S. A., Hollis, B. R., Liechty, D. S., Hamilton II, H. H., & Mersk, N. R. (2001). X-33 experimental aeroheating at mach 6 using phosphor thermography. *Journal of Spacecrafts and Rockets*, *38*(5). https://doi.org/10.2514/2.3748

Hung, C. M., & Buning, P. G. (1985). Simulation of blunt-fin-induced shock-wave and turbulent boundary-layer interaction. *Journal of Fluid Mechanics, 154*(1), 163–185. https://doi.org/10.1017/S0022112085001471

Knight, D. D., & Badekas, D. (1992). Quasiconical flowfield structure of the three-dimensional single fin interaction. *AIAA Journal, 30*(12), 2902–2904. https://doi.org/10.2514/3.48972

Kolesnik, E. V., & Smirnov, E. M. (2021). Supersonic laminar flow past a blunt fin: Duality of the numerical solution. *Technical Physics, 66*(6), 741–748. https://doi.org/10.1134/S1063784221050133

Kolesnik, E. V., & Smirnov, E. M. (2023). Duality of the stream pattern of supersonic viscous gas flow past a blunt-fin junction: The effect of a low sweep angle. *Fluid Dynamics, 58*(1), 18–28. https://doi.org/10.1134/S0015462822601887

Kolesnik, E. V., & Smirnov, E. M. (2024). *Dual numerical solutions for a supersonic laminar flow past a plate and a blunt-fin body junction*. AIP Conference Proceedings, 2351, 040030. https://doi.org/10.1063/5.0052221

Kolesnik, E., Smirnov, E., & Babic, E. (2023). Dual numerical solution for 3D supersonic laminar flow past a blunt-fin junction: Change in temperature ratio as a method of flow control. *Fluids, 8*(5), 149. https://doi.org/10.3390/fluids8050149

Mortazavi, M., & Knight, D. (2017). *Shock wave laminar boundary layer interaction at a hypersonic flow over a blunt fin-plate junction.* Proceedings of the 55th American Institute of Aeronautics and Astronautics Aerospace Sciences Meeting (Paper No. 0536). https://doi.org/10.2514/6.2017-0536

Narayan, A., Narayanan, S., & Kumar, R. (2017). Hypersonic flow past nose cones of different geometries: A comparative study. *Simulation: Transactions of the Society for Modeling and Simulation International, 24*(8), 675–686. https://doi.org/10.1177/0037549717733051

Ngoh, H., & Poggie, J. (2022). Forced separation unsteadiness in a supersonic blunt fin flow. *Physical Review Fluids, 7*, 093903. https://doi.org/10.1103/PhysRevFluids.7.093903

Poggie, J., & Smits, A. J. (1997). Wavelet analysis of wall-pressure fluctuations in a supersonic blunt-fin flow. *AIAA Journal, 35*(10), 1641–1647. https://doi.org/10.2514/2.18

Sedney, R., & Kitchens Jr, C. W. (1975). *The structure of three-dimensional separated flows in obstacle-boundary layer interactions.* USA Ballistic Research Laboratories. Retrieved from https://apps.dtic.mil/sti/pdfs/ADA011254.pdf

Song, J. W., Yu, M. S., & Cho, H. H. (2007). Heat transfer near sharp and blunt fins protruded in a supersonic flow. In *Proceedings of the 39th AIAA Thermophysics Conference*. https://doi.org/10.2514/6.2007-4151

Sydney, R., & Kitchens, C. W. Jr. (1977). *Separation ahead of protuberances in supersonic turbulent boundary layers*. USA Ballistic Research Laboratory. https://doi.org/10.2514/3.60658

Viswanath, P. R. (1988). Shock-wave-turbulent-boundary-layer interaction and its control: A survey of recent developments. *Indian Academy of Sciences, 12*(1 & 2), 45–104. https://link.springer.com/article/10.1007/BF02745660#citeas

Wang, S. F., Ren, Z. Y., & Wang, Y. (1998). Effects of Mach number on turbulent separation behaviours induced by blunt fin. *Experiments in Fluids, 25*(4), 347–351. https://doi.org/10.1007/s003480050239

Weng, Y., Li, Q., Tan, G., Su, W., & You, Y. (2024). Numerical investigations on interactions between 2D/3D conical shock wave and axisymmetric boundary layer at Mach 2.2. *Aerospace Science and Technology, 144*(3), Article 108769. https://doi.org/10.1016/j.ast.2023.108769

Xiao, F., Li, Z., Zhang, Z., Zhu, Y., & Yang, J. (2018). Hypersonic shock wave interactions on a V-shaped blunt leading edge. *AIAA Journal, 56*(1), 220–230. https://doi.org/10.2514/1.J055915